Al-Qadisiyah JournalFor Engineering Sciences 19 (2026) 164 – 169

Contents lists available at: http://qu.edu.iq

Al-Qadisiyah Journal for Engineering Sciences

Journal homepage: https://qjes.qu.edu.iq

Research Paper

Study of 3D-printed honeycomb orientation on vibration energy harvesting

Nicholas T. Yong [1,2], ***and Choon L. Hoo*** [3]

[1]School of Engineering and Physical Sciences, Heriot-Watt University Malaysia, 62200 Putrajaya, Malaysia.
[2]ARRK Asia, Block E-10-01, Oasis Ara Damansara, Jalan PJU 1A/7, Ara Damansara, 47301 Petaling Jaya, Malaysia.
[3]School of Engineering, Faculty of Engineering and Technology, Sunway University, Malaysia.

ARTICLE INFO

Article history:
Received 05 May 2025
Received in revised form 18 February 2026
Accepted 06 June 2026

keyword:
Hexagonal
Fused deposition modeling
Cantilever beam
Thickness
Natural frequency

ABSTRACT

With the advances in technology, sustainable renewable energy implementation in many applications is becoming important, such as in wireless sensors. Vibration energy harvesting can convert environmental mechanical vibration into useful energy. Honeycomb core structure has shown promising results in cantilever dynamic vibration. However, there is a limited study on its structural variation. This research focuses on different beam thickness and angle orientation of 3D printed hexagonal core structure to improve vibrational cantilever energy harvesting. The beam thickness was studied at 4 *mm*, 6 *mm*, and 8 *mm* with re-oriented honeycomb core at 0°and 30°. The test rig was modelled as a mass-spring system. The model was simulated for modal analysis and power generation with piezoelectric. The natural frequencies and vibration amplitudes were compared between simulation and experimentation with a vibrational shaker machine and a data acquisition device. The results showed that the 30°honeycomb core has better dynamical amplitudes and energy harvesting as compared to the conventional 0°honeycomb core beam. The different beam thicknesses affect the beam stiffness and, therefore, vary the vibrational amplitude and generated power. The 30°core with lower thickness was found to have the highest power generation due to the better distribution of stress along the beam.

1. Introduction

Energy plays an important role in various ranges of industrial applications and development. With the alarming depletion of non-renewable energy sources, research has been studying the implementation of renewable energy to provide a greener environment for future generations [1]. Vibrational piezoelectric energy harvesters are promising keys in creating sustainable energy generation technologies through harvesting environmental and ambient vibrational mechanical energy, such as buildings, machinery, and human activities. Thoroughly converting the unused environmental vibrational energy source into electrical energy [2]. In recent years, more wireless monitoring systems have been implemented to monitor the structural condition in buildings and bridges [3, 4]. The wireless sensors were powered by small batteries to detect crack propagation within structures [5]. Such systems encountered an inaccessible battery replacement. Therefore, energy harvesting has gained much interest in creating a sustainable energy supply for low-powered devices in remote areas [6]. A vibrational piezoelectric energy harvester is one of the common harvesting mechanisms. The operating bandwidth of the ambient frequency shall match the natural frequency of the system to increase its efficiency. The vibrational energy harvester [7] utilises the piezoelectric effect to convert the ambient mechanical vibrational kinetic energy into electrical energy to power small devices or store in a battery. The piezoelectric effect generates an electric field through the Quartz crystals with mechanical stress, such as deformation on an object or vice versa. Various man-made piezoelectric materials, such as polymers and ceramics, have been developed. Ceramic-type piezoelectric commonly has a higher piezoelectric constant, which corresponds to higher direct piezoelectric output but comes with lower ductility and flexibility [8], in contrast to polymer-based piezoelectric material. In general, piezoelectric energy harvesting possesses high power density and versatility with simple power generation operation. Electrical energy generation through piezoelectric relies on the vibration frequency, displacement, and resonance frequency [9]. Although piezoelectricity has its disadvantages, improvement can be made by increasing its non-linearity and frequency up-conversion. Additive manufacturing promotes rapid prototyping with customisability traits. The common printing materials consist of polylactic acid (PLA) and acrylonitrile-butadiene styrene (ABS). Fuse Deposition Modelling (FDM) 3D printing in manufacturing a vibrational energy harvester beam allows design flexibility. With rapid prototyping, complex structures such as honeycomb cellular beams can be easily fabricated for various vibrational energy harvesting studies. Honeycomb shapes have been proven to offer a high strength-over-weight ratio, lightweight, and great energy absorption [10]. A recent study [11] studied the effect from multilayer configuration. The multilayer honeycomb core structure could provide a higher amplitude-to-weight ratio. This research focuses on the effect of different structural approaches on 3D printed vibrational beams to improve vibrational piezoelectric cantilever beam energy harvesters. The dynamic performance, such as the natural frequency and vibrational amplitude, and power generation through variation of beam thickness and hexagonal cellular core orientation angles, will be studied.

2. Methodology

2.1 Mathematical modeling

The cantilever system was modelled as a mass-spring-damper system with base excitation. The general form of the equation of motion is given by Eq. 1, where m, k, and c are mass, stiffness, and damping constant respectively.

*Corresponding Author.
E-mail address: stevenhoo@sunway.edu.my ; Tel: (+60) 12-347 7161 (Choon Hoo)

https://doi.org/10.30772/qjes.2025.165746.1764

Nomenclature

c	Damping constant (Ns/m)
c_p	Capacitance (F)
D	Electric displacement (C/m^2)
d	Dielectric constant
E	External electrical field (V/m)
E^{eff}	Effective tensile modulus (MPa)
E_s	Overall effective tensile modulus (MPa)
G^{eff}	Effective shear modulus (MPa)
h	Core side length (mm)
k	Stiffness (N/m)
l	Core incline side length (mm)
m	Mass (kg)
P_{avg}	Maximum piezoelectric average power (W)
R	Resistance (Ω)
S	Polarization area (m^2)
T	Stress (MPa)
Greek Symbols	
ε	yyyyyyyyy
θ	yyyyyyyyy
x	Mass displacement (m)
y	Excitation displacement (M)

$$m\ddot{x}+c(\dot{x}-\dot{y})+k(x-y)=0 \tag{1}$$

The beam vibrational amplitude will be determined from the response power spectral density (PSD). The corresponding frequencies, f were obtained with Eq. 2 through the random vibration analysis [12].

$$Amplitude=\sqrt{PSD\times f}\ \ (m) \tag{2}$$

The theoretical piezoelectric energy output is found through the direct piezoelectric effect Eqs. 3 and 4 [13], where D, d, ε, T and E are the electric displacement, dielectric constant, piezoelectric strain, stress, and external electrical field, respectively. The maximum piezoelectric average power, P_{avg} can be determined in Eq. 4 where S, c_p, and R are the polarization area, capacitance of the piezoelectric material, and resistance, respectively. Given the material specification in Table 1.

Table 1. PLA material.

Mechanical properties	Values
Density	1250 kg/m^3
Isotropic Thermal Conductivity	0.144 $J/(C\ m\ s)$
Isotopic Resistivity	4.31 x 109 Ωm
Young's Modulus	3.45 GPa
Poisson's Ratio	0.39
Shear Modulus	1.241 GPa

The mechanical properties related to the dynamic motion of the system, such as the elastic properties (effective tensile modulus, E_{eff}, effective shear modulus, G_{eff} and effective Poisson's ratios, v_{eff}) of the hexagonal core structure can be determined from Eqs. 5, 6, 7, 8, 9, 10 and 11 [14] as shown in Table 2.

$$D_m=d_{mi}T_i+\varepsilon^T_{mk}E_k\ \ (C/m^2) \tag{3}$$

$$P_{avg}=\frac{1}{8}\left(\frac{DTS}{c_p}\right)^2\frac{1}{R}\ \ (W) \tag{4}$$

$$E_1^{eff}=E_s\frac{1}{8}\left(\frac{t}{l}\right)^3\frac{\frac{h}{l}+sin(\theta)}{cos^3(\theta)}\ \ (MPa) \tag{5}$$

$$E_2^{eff}=E_s\frac{1}{8}\left(\frac{t}{l}\right)^3\frac{cos(\theta)}{sin^2(\theta)\left(\frac{h}{l}+sin(\theta)\right)}\ \ (MPa) \tag{6}$$

$$E_3^{eff}=E_s\frac{\left(\frac{h}{l}+2\right)\frac{t}{l}}{2cos(\theta)\left(\frac{h}{l}+sin(\theta)\right)}\ \ (MPa) \tag{7}$$

$$G_{12}^{eff}=G_s\left(\frac{t}{l}\right)^3\frac{\left(\frac{h}{l}+sin(\theta)\right)}{\left(\frac{h}{l}\right)^2\left(1+2\frac{h}{l}\right)cos(\theta)}\ \ (MPa) \tag{8}$$

$$G_{13}^{eff}=G_s\frac{\frac{t}{l}cos(\theta)}{\frac{h}{l}+sin(\theta)}\ \ (MPa) \tag{9}$$

$$v_{12}^{eff}=\frac{cos^2(\theta)}{sin(\theta)\left(\frac{h}{l}+sin(\theta)\right)}\ \ (MPa) \tag{10}$$

$$v_{21}^{eff}=\frac{sin(\theta)\left(\frac{h}{l}+sin(\theta)\right)}{cos^2(\theta)}\ \ (MPa) \tag{11}$$

Table 2. Design parameters of beam.

Mechanical properties	Values
E_1^{eff}	20.01 (MPa)
E_2^{eff}	20.01 (MPa)
E_3^{eff}	67.55 (MPa)
G_{12}^{eff}	3.75 (MPa)
G_{13}^{eff}	16.9 (MPa)
v_{12}^{eff}	0.45
V_{21}^{eff}	0.45

Figure 1 shows the schematic diagram of the 0° and 30° hexagonal core unit cell with the geometric parameters t, l, h and θ.

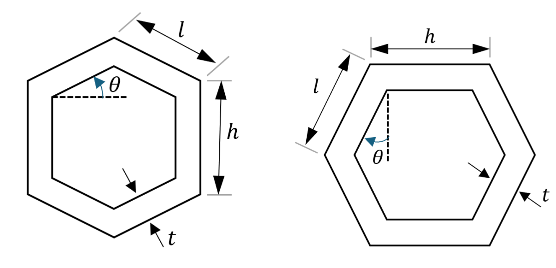

(a) Model of 0°hexagonal core. (b) Model of 30°hexagonal core.

Figure 1. Schematic of dimensional representation of unit cells.

2.2 Beam design and prototyping

The study implements 0° and 30° hexagonal core orientations to give a distinct symmetrical difference, as the geometrical shape will repeat itself due to a regular hexagon shape. The hexagonal core had a 2 mm wall thickness, with 8 mm and 6 mm of outer and inner hexagon side respectively. While 0° hexagon core has a 16 mm total width and 14 mm height, the 30° hexagon core has the opposite dimensions of 16 mm height and 14 mm total width. Figures 2a and 2b show the Inventor Computer-Aided Drawing (CAD) models of beam design with 0° and 30° orientation, respectively. Both orientation of beam designs has a length of 100 mm to width or 50 mm (ratio of 2:1). The beam thicknesses will vary from 4 mm to 8 mm. A total of 6 samples were studied in this research, as listed in Table 3.

Table 3. Design samples of vibrational beam.

Core orientation (°)	Wall thickness (mm)
0	4, 6, 8
30	4, 6, 8

The beam samples were 3D printed in a FDM Ultimaker 3 with a 0.4 mm nozzle, polylactic acid (PLA) printing material with an infill density of a 50%, infill. Figures 3a and 3b show the top and side view respectively of 3D printed beam with 8 mm beam thickness and 0° orientation.

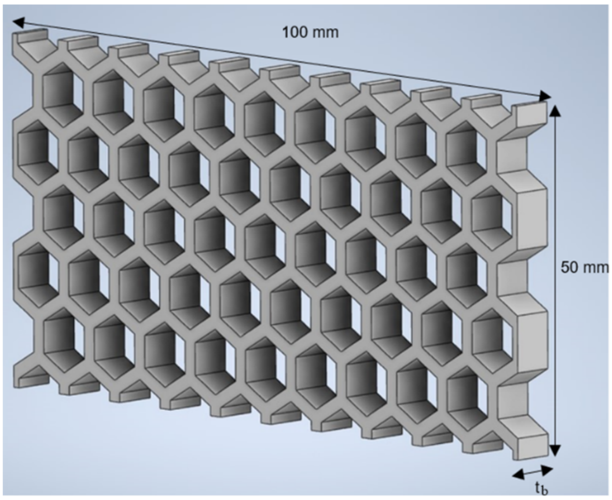

(a) CAD model of honeycomb with a core beam orientation of 0°.

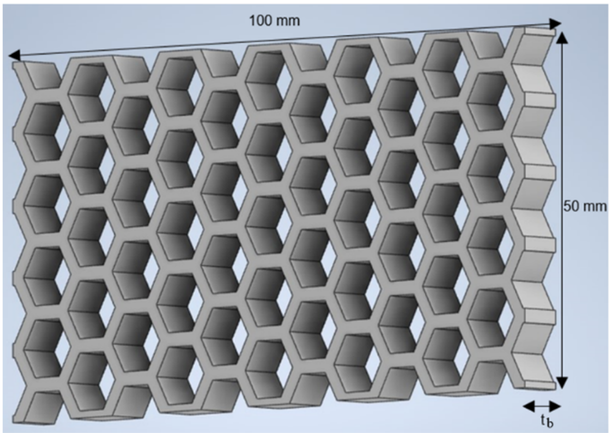

(b) CAD model of honeycomb with a core beam orientation of 30°.

Figure 2. CAD model of honeycomb with a two cores beam orientation.

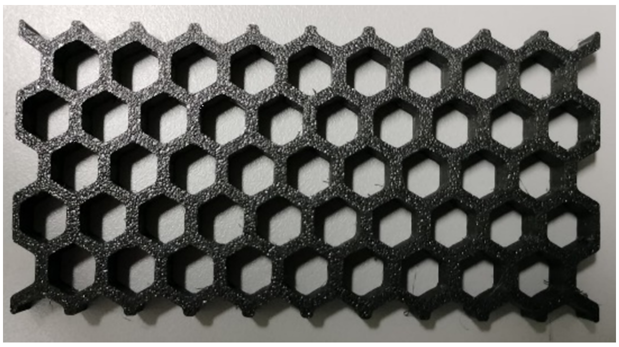

(a) Top view of a testing model.

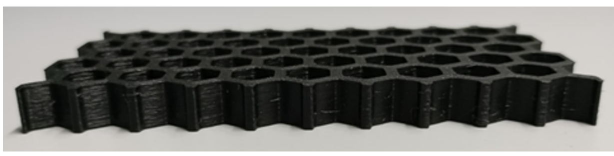

(b) Side view Model of a testing model.

Figure 3. Typical of 3D printed 8 *mm* thick of 0°core beam.

2.3 Simulation analysis

Figure 4 shows the vibrational beam simulation analysis using the ANSYS software. The model boundary was set as a cantilever beam model. One end of the beam is set to vibrate with a vertical acceleration of $0.1g$. The PLA material properties are set as input, and the meshing is generated with $800\mu m$ element size. The first six mode shapes were generated by ANSYS to identify the natural frequencies of the beam Table 4, which were later used for random vibration analysis through the Power Spectral Density (*PSD*) G-acceleration tool. The G-acceleration value will be determined using Eq. 12 and used in the response PSD tool to plot the amplitude over frequency graph. Finally, the piezoelectric energy generation can also be simulated in ANSYS. A piezoelectric sensor with specifications stated in Table 5 is placed on the beam tip. The piezoelectric film is made of lead zirconate titanate material (PZT) with a Resonant frequency of 45 Hz. The piezoelectric film has a length of 30 *mm* and a width of 15 *mm*.

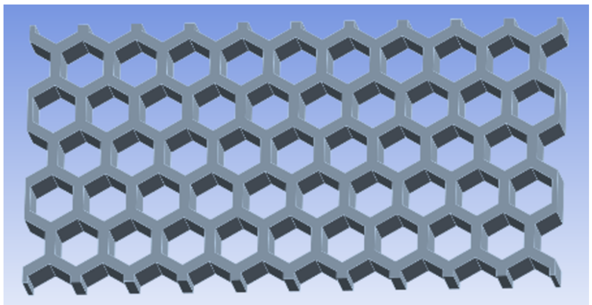

Figure 4. Ansys CAD model of honeycomb simulation.

Table 4. Data of the first 6 mode shapes of 8 *mm* thick 30°core beam.

Mode	Frequency, Hz
1	105.9
2	380.51
3	409.63
4	640.71
5	1222.9
6	1523.7

Table 5. Piezoelectric film specification.

Parameters	PZT
Thickness, t	28 μm
Piezo strain constant	
d_{31}	$23 \times 10^{-12}\ CN^{-1}$
d_{33}	$-33 \times 10^{-12}\ CN^{-1}$
Piezo stress constant	
g_{31}	$216 \times 10^{-3}\ VmN^{-1}$
g_{33}	$-330 \times 10^{-3}\ VmN^{-1}$
Electromechanical coupling factor, k_t	14%
Capacitance, C	380 F
Young's Modulus, E	$2 \times 10^{9}\ Nm^{-2}$

$$G\,Acceleration = \frac{Load\ \ Acceleration}{Frequency} \tag{12}$$

2.4 Experimental setup

Figure 5 shows the experiment setup for the vibration testing of a cantilever beam with the 3D printed honeycomb beams. The shaker machine will produce vibration to simulate the ambient vibration from the environment. The load acceleration is set as 0.1 g, similar to the ANSYS simulation parameter. An infrared sensor is placed directly on top of the beam tip to measure the beam vibrational amplitude, which is later processed in the LabVIEW software.

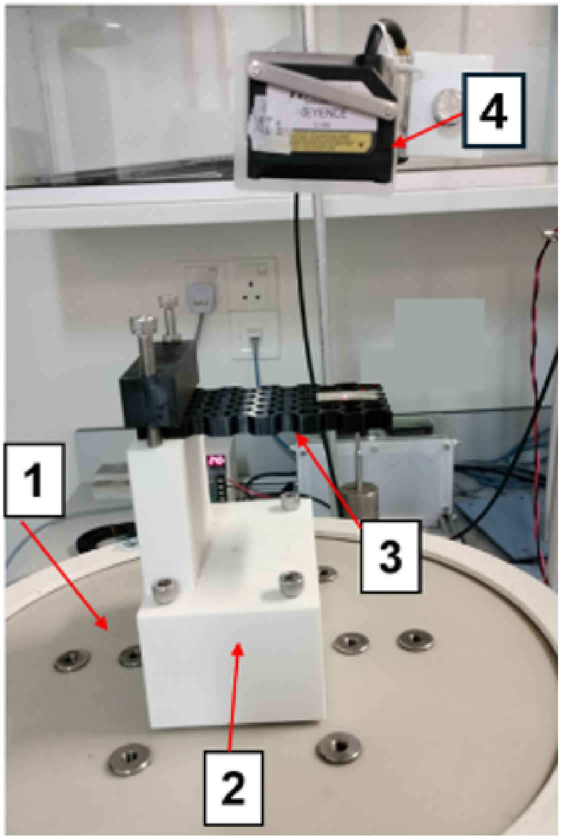

Figure 5. Experimental setup: (1) shaker, (2) clamp, (3) 3D printed beam, and (4) infrared sensor.

3. Results and Discussion

The simulation and experimental results have been collected for two core orientations (0° and 30°) with varying beam thickness from 4 mm to 8 mm beams to investigate the mode shapes, dynamical amplitude, and power generation and Table 6 summaries the simulation data.

Table 6. Mode shapes data.

Thickness(mm)	Modes	Natural frequency (Hz)	
		0°	30°
4	1^{st}	63.183	60.347
	2^{nd}	241.03	237.96
	3^{rd}	389.99	373.45
6	1^{st}	88.172	83.805
	2^{nd}	314.51	312.12
	3^{rd}	465.05	407.22
8	1^{st}	112.22	105.9
	2^{nd}	382.12	380.51
	3^{rd}	467.55	409.63

3.1 Modal analysis

Table 5 shows the first three mode shapes from the ANSYS modal analysis simulation. The increase of beam thickness increases the natural frequency of the beam, with the largest first mode natural frequency found at 8 mm in both core orientations. The 30° core beams always had a lower natural frequency compared to the 0° core beams. Increasing thickness and 0° core arrangement provide higher stiffness to the overall beam structure, which corresponds to the higher natural frequency.

3.2 Dynamic performance

Figure 6a shows the simulation and experimental dynamical amplitude for a beam thickness of 4 mm at 0° core beam. The simulation amplitude reaches around 3.87 mm at a natural frequency of 63.2 Hz, as compared to the experimental amplitude of 4.07 mm at a natural frequency of 62.8 Hz. The experimental amplitude is higher, but with a lower natural frequency. In the meantime, Fig. 6b shows the response for a 4 mm beam thickness at 30° core orientation. The experimental amplitude is larger (4.40 mm) than the simulation amplitude (3.80 mm). Both natural frequencies were recorded at 60 Hz. A similar trend was observed for 6 mm and 8 mm beam thicknesses.

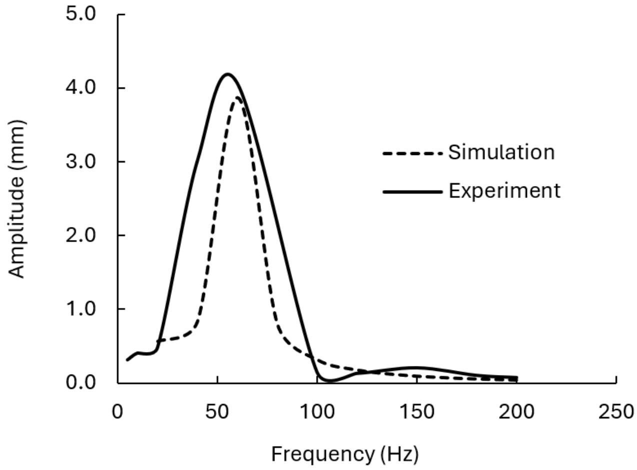

(a) Model of 0°hexagonal core.

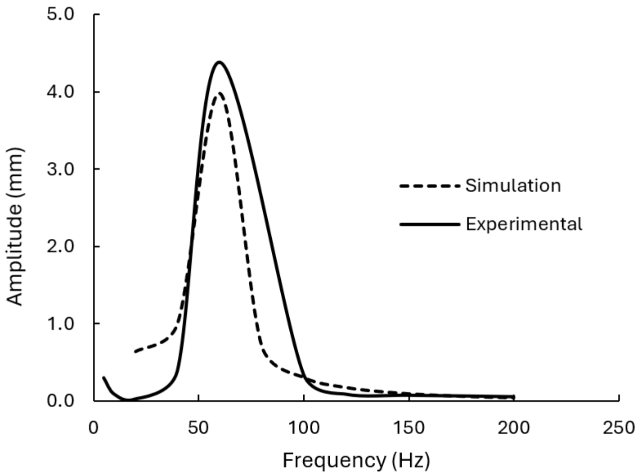

(b) Model of 30°hexagonal core.

Figure 6. Simulation and experimental vibrational amplitude for 4 *mm* testing model.

Figure 7 shows the experimental dynamical amplitudes comparison between the cores. The result illustrates that increasing the beam thickness will increase the natural frequency but lower the amplitude. Regardless of the beam thickness, 30° core will always have larger amplitudes. Table 7 summarises the simulation and experimental findings. The power generation for both core orientations decreases with increasing beam thickness. The 30° core orientation has higher power generation compared to 0° core orientation, with 4 mm beam thickness being the highest compared to other thicknesses. This corresponds to the higher amplitude in 30° core orientation. Knowing that the vibration system is modelled as a mass-spring system, the beam deflection decreases with increasing stiffness of the spring (beam) [15]. Changes in stiffness affect the mass variable and the system's natural frequency. Since beam deflection is proportional to the electrical output produced by the piezoelectric layer [16], beam thickness has an inverse correlation with power generation. The 30° core beam has better performance due to having a well-distributed stress along the beam, which is supported by Yang and Cao [13] who studied the stress impact on piezoelectric power generation. Table 7 also shows the error analysis on the simulation and experimental differences for the natural frequency and vibration amplitude. The % error for natural frequency is lower than 0.6%. The amplitude error is slightly higher due to micro-slip of the cantilever setup during experimentation, and also the lower experimental natural frequency would allow vibration excitation closer to the potential resonance range and therefore higher dynamical vibration response.

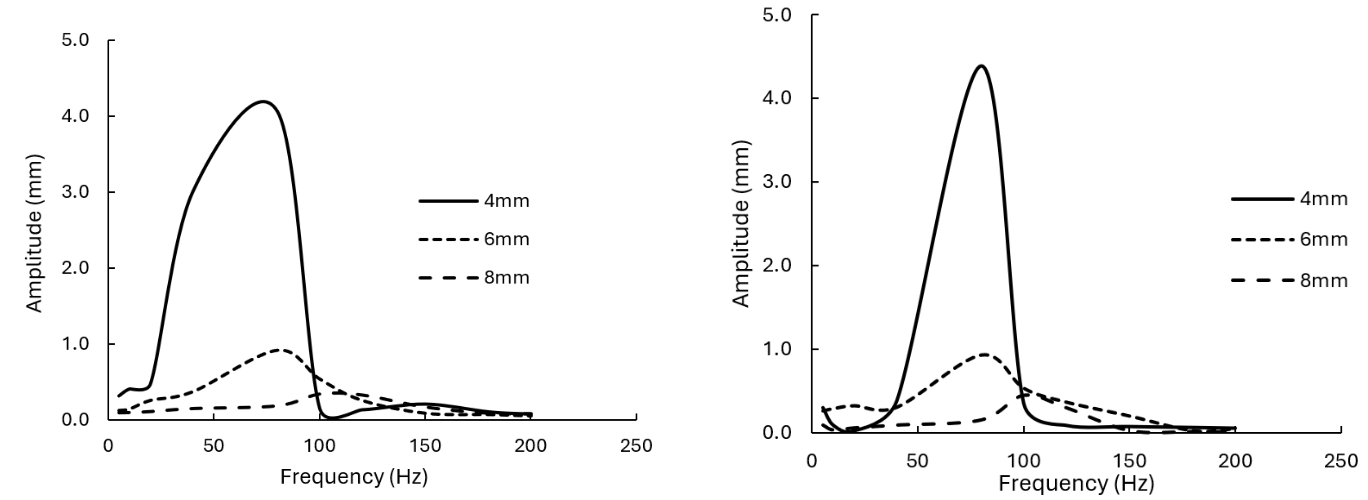

(a) Model of 0°hexagonal core.

(b) Model of 30°hexagonal core.

Figure 7. Experimental vibrational amplitudes for different beam thicknesses model.

Table 7. Natural frequencies and dynamical amplitudes.

Thickness (mm)	Ansys Frequency Hz		Exp. Frequency Hz		Frequency Error%		Peak Simulation Amplitude (mm)		Peak Experimental Amplitude (mm)		Amplitude Error %		Peak Simulation Power (mW)	
	0°	30°	0°	30°	0°	30°	0°	30°	0°	30°	0°	30°	0°	30°
4	063.183	060.347	062.810	060.447	0.59	0.17	03.872	03.983	04.064	04.384	04.96	10.07	0.0520	0.0630
6	088.172	083.805	088.101	083.725	0.08	0.10	00.855	00.876	00.912	00.931	06.67	06.28	0.0045	0.0046
8	112.220	105.900	111.820	105.670	0.36	0.22	00.322	00.425	00.341	00.448	05.90	05.41	0.00011	0.0002

4. Conclusions

FDM 3D printed honeycomb core structure was studied to improve energy harvesting. The investigation focused on the effect of varying beam thickness and orientation of the honeycomb core structure on dynamical amplitude and energy generation performance. The cantilever beam system was modelled as a mass-spring system for modal analysis and piezoelectric energy generation. The simulation findings were verified through a vibrational shaker experiment. Two distinct honeycomb core orientations of the beam were investigated, where the 30° showed a uniform stress distribution along the beam. The 30° core beam performed better than the 0° core beam with higher vibrational amplitudes and power generation. Increasing the beam thickness will increase the stiffness of the beam. This leads to a smaller amplitude, which eventually gives lower power generation. The 30° core with 4 mm beam thickness has the best performance in dynamical amplitude and energy generation. In the future, the study can be extended to different angles of orientation to manipulate the stress distribution within the beam. This work may identify the optimum position for best power generation. A multilayer beam can also be explored since it has been shown to improve the amplitude-to-weight ratio, which should amplify the power generation further.

Authors' contribution

All authors contributed equally to the preparation of this article.

Declaration of competing interest

The authors declare no conflicts of interest.

Funding source

This work was supported by the Ministry of Higher Education (MOHE) Malaysia through the Fundamental Research Grant Scheme (FRGS/1/2021/TK0/HWUM/02/1).

Data availability

The data that support the findings of this study are available from the corresponding author upon reasonable request.

Acknowledgements

The authors would like to acknowledge that this study was supported by the Ministry of Higher Education (MOHE) Malaysia.

REFERENCES

[1] N. F. Yah, A. N. Oumer, and M. S. Idris, "Small scale hydro-power as a source of renewable energy in malaysia: A review," *Renewable and Sustainable Energy Reviews*, vol. 72, pp. 228–239, 2017. [Online]. Available: https://doi.org/10.1016/j.rser.2017.01.068

[2] Z. Zhang, S. Lin, Y. Gu, L. Zhang, S. Wang, S. Zhai, and J. Kan, "Design and characteristic analysis of a novel deformation-controllable piezoelectric vibration energy harvester for low frequency," *Energy Conversion and Management*, vol. 286, pp. 117 016–117 016, 2023. [Online]. Available: https://doi.org/10.1016/j.enconman.2023.117016

[3] A. Marin, J. Turner, D. S. Ha, and S. Priya, "Broadband electromagnetic vibration energy harvesting system for powering wireless sensor nodes," *Smart Materials and Structures*, vol. 22, no. 7, p. 075008, 2013. [Online]. Available: https://doi.org/10.1088/0964-1726/22/7/075008

[4] A. Mouapi, N. Hakem, N. Kandil, and G. V. Kamani, "Energy harvesting design for autonomous wireless sensors network applied to trains," *2017 IEEE International Ultrasonics Symposium (IUS)*, pp. 1–4, 2016. [Online]. Available: https://doi.org/10.1109/ULTSYM.2016.7728636

[5] L. Qi, H. Pan, Y. Pan, D. Luo, J. Yan, and Z. Zhang, "A review of vibration energy harvesting in rail transportation field," *IScience*, vol. 25, no. 3, p. 103849, 2022. [Online]. Available: https://doi.org/10.1016/j.isci

[6] M. Peigney and D. Siegert, "Low-frequency electromagnetic energy harvesting from highway bridge vibrations," *Journal of Bridge Engineering*, vol. 25, no. 8, p. 04020056, 2020. [Online]. Available: https://doi.org/10.1061/(asce)be.1943-5592.0001581

[7] S. Katzir, "The discovery of the piezoelectric effect," *Archive for History of Exact Sciences*, vol. 57, no. 1, pp. 61–91, 2003. [Online]. Available: https://doi.org/10.1007/s00407-002-0059-5

[8] A. Megdich, M. Habibi, and L. Laperrière, "A review on 3d printed piezoelectric energy harvesters: Materials, 3d printing techniques, and applications," *Materials Today Communications*, vol. 35, p. 105541, 2023. [Online]. Available: https://doi.org/10.1016/j.mtcomm.2023.105541

[9] C. Covaci and A. Gontean, "Piezoelectric energy harvesting solutions: A review," *Sensors*, vol. 20, no. 12, p. 3512, 2020. [Online]. Available: https://doi.org/10.3390/s20123512

[10] J. Zhou, H. Liu, J. P. Dear, B. G. Falzon, and Z. Kazancı, "Comparison of different quasi-static loading conditions of additively manufactured composite hexagonal and auxetic cellular structures," *International Journal of Mechanical Sciences*, vol. 244, p. 108054, 2023. [Online]. Available: https://doi.org/10.1016/j.ijmecsci.2022.108054

[11] R. Q. Tan, C. L. Hoo, C. H. Lai, and F. M. Foong, "Study of honeycomb layering in multi-plane configuration for vibrational energy harvesting," *International Journal of Mechanical Engineering and Robotics Research*, vol. 13, no. 5, pp. 530–534, 2024. [Online]. Available: https://doi.org/10.18178/ijmerr.13.5.530-534

[12] H. M. Gomes, D. dos Santos Gaspareto, F. de Souza Ferreira, and C. A. K. Thomas, "A simple closed-loop active control of electrodynamic shakers by acceleration power spectral density for environmental vibration tests," *Experimental Mechanics*, vol. 48, no. 5, pp. 683–692, 2008. [Online]. Available: https://doi.org/10.1007/s11340-008-9134-4

[13] H. Yang and D. Cao, "An investigation on stress distribution effect on multi-piezoelectric energy harvesters," *Frontiers of Structural and Civil Engineering*, vol. 11, no. 3, pp. 301–307, 2017. [Online]. Available: https://doi.org/10.1007/s11709-017-0404-z

[14] N. Chandrasekharan and L. L. Thompson, "Increased power to weight ratio of piezoelectric energy harvesters through integration of cellular honeycomb structures," *Smart Materials and Structures*, vol. 25, no. 4, p. 045019, 2016. [Online]. Available: https://doi.org/10.1088/0964-1726/25/4/045019

[15] D. D. Sivan and Y. M. Ram, "Mass and stiffness modifications to achieve desired natural frequencies," *Communications in Numerical Methods in Engineering*, vol. 12, no. 9, pp. 531–542, 1996.

[16] M. Rafiee, J. Yang, and S. Kitipornchai, "Large amplitude vibration of carbon nanotube reinforced functionally graded composite beams with piezoelectric layers," *Composite Structures*, vol. 96, pp. 716–725, 2013. [Online]. Available: https://doi.org/10.1016/j.compstruct.2012.10.005

How to cite this article:
Nicholas T. Yong and Choon L. Hoo (2026). 'Study of 3D-printed honeycomb orientation on vibration energy harvesting', Al-Qadisiyah Journal for Engineering Sciences, 19(2), pp. 164- 169. https://doi.org/10.30772/qjes.2025.165746.1764